

# A Quantum Router Architecture for High-Fidelity Entanglement Flows in Multi-User Quantum Networks

Yuan Lee, Eric Bersin, Axel Dahlberg, Stephanie Wehner, Dirk Englund  
 (Dated: November 9, 2021)

The distribution of quantum entanglement between remote clients offers opportunities for secure communication, distributed quantum computation, and quantum-enhanced sensing. A key technology for allowing such a quantum network to extend over large distances is the quantum repeater, which typically employs a long-lived quantum memory with an optical interface. The past decade has seen tremendous progress in experimentally realizing the fundamental building blocks of these repeaters, but open questions remain on what architectures achieve optimal entanglement flows in multi-user quantum networks. Here, we propose a quantum router architecture comprising many quantum repeater nodes in a flexible photonic switchboard architecture to broker entanglement flows across such networks. We compute the rate and fidelity of entanglement distribution using this architecture using an event-based simulation platform. We find that the router's photonic switchboard improves the entanglement fidelity with the number of qubits per node, without a significant drop in the entanglement distribution rate. The proposed quantum router architecture uses present-day photonic switch technology such as photonic integrated circuits, opening a path to near-term deployable multi-user quantum networks.

## I. INTRODUCTION

Quantum networks distribute quantum information to enable the realization of tasks that are intractable for their classical counterparts. Key to these applications is the sharing of entanglement between many users over large distances, allowing quantum key distribution, distributed quantum computing, and quantum-enhanced sensing. While entanglement distribution has been demonstrated over short distances [1], long-distance quantum networking is hampered by the exponential loss of photons in optical fibers [2]. Quantum repeaters [3] can overcome this problem by forming chains of entangled nodes.

Figure 1a shows a link layer schematic of such a repeater-connected quantum network. A graph of quantum repeaters connected by “quantum links” forms the backbone of the network. “Client” nodes connect to the network through their nearest “repeater” node, facilitating the sharing of entanglement between clients. Hidden under the link layer abstraction lies a physical layer of repeater devices and lossy “quantum channels”, as depicted in Fig. 1b. A typical repeater device consists of a memory capable of generating and storing entanglement with a photonic mode. The entanglement scheme used in a link between two repeater nodes determines the devices and channels used in the physical layer. Nitrogen vacancy (NV) centers in diamond have been entangled at a distance of 1.3 km [1] using the scheme proposed by Barrett and Kok [4], which uses a 50:50 beamsplitter to erase which-path information and detectors to herald entanglement. A related scheme proposed by Cabrillo [5] was used to provide on-demand entanglement between NV centers using a phase-stabilized fiber link [6]. Recently, the direct-transmission bound for quantum communication was broken [7] using a scheme proposed by Duan and Kimble [8], which relies on scattering photons from spins in high-cooperativity cavities. These protocols are

all inherently probabilistic, such that a single attempt at distributing entanglement succeeds with probability  $p_{\text{distant}}$ .

While the finite bandwidth of these memories can limit entanglement generation rates, multiplexed architectures [9, 10] have been proposed to increase these rates. Here, we introduce a quantum router architecture that uses multiplexing and high local connectivity (a “photonic switchboard”) to improve the rate and the fidelity of entanglement distribution. The router uses local, low-loss connections to link Alice’s and Bob’s entangled qubits, thereby establishing entanglement across the channel. This quantum router architecture is motivated by recent advances in integrated photonics, with demonstrations of fast and low-loss on-chip switching [11] of many photonic modes and the integration of quantum emitters with integrated circuits [12].

## II. RESULTS

### A. Router Architecture

We analyze the performance of our quantum router proposal for the NV center in diamond as the qubit platform and the Barrett-Kok [4] scheme as the entanglement protocol. However, our architecture is agnostic to the specific memory and entanglement-generation protocol.

In Fig. 2, we show the connectivity between photonic and stationary qubits in a standard multiplexed repeater considered for diamond color centers [14] (a) and a multiplexed repeater with a router (b). In this representation, each qubit register within the router is linked by a distinct mode to a corresponding register at an adjacent neighboring node, here labelled left and right for generality. Different modes are shown separately, though they may be transmitted through the same physical channel. Each qubit register comprises a single NV center

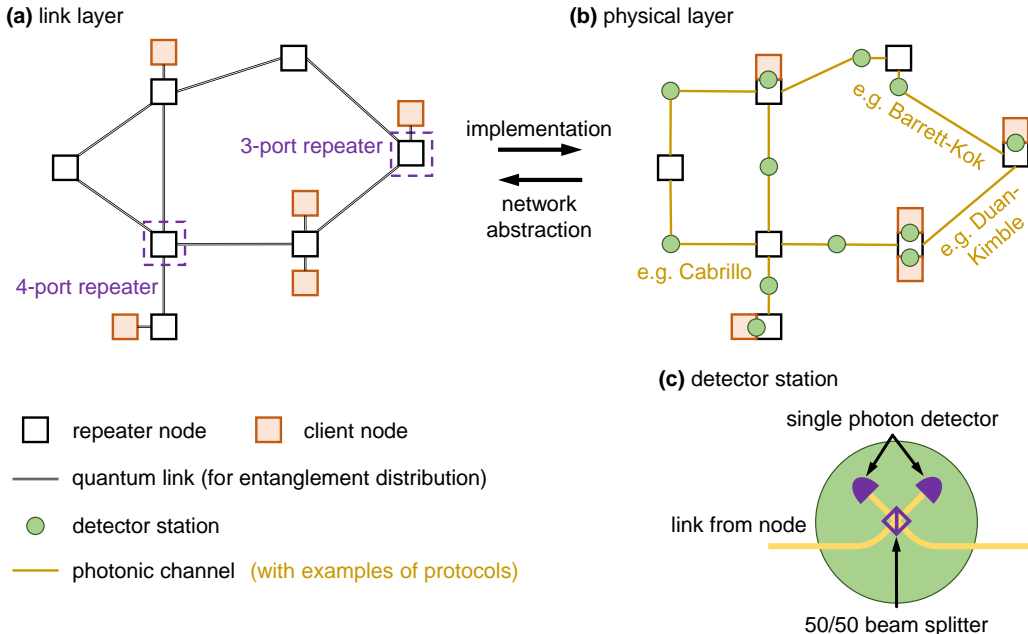


FIG. 1. Components of a quantum repeater network. **(a)** The link layer [13] enumerates connections enabling entanglement between nodes in the network. The quantum network comprises client nodes, which end users directly access, and repeater nodes, which connect clients by propagating entanglement through the network. We classify repeater nodes based on the number of other nodes they connect to: a 4-port and a 3-port repeater are labeled. **(b)** In the physical layer, repeater nodes may be connected by a variety of entanglement protocols. While all protocols require transmission of an entangled photon through a photonic channel, the specific protocol used in each link determines the physical configuration of these channels (e.g. optical fibers) and measurement devices associated with that link. Possible protocols include the cavity-mediated Duan-Kimble protocol [8] and the photon emission-based Barrett-Kok [4] and Cabrillo [5] protocols. These latter protocols employ an intermediate detector station between nodes to herald successful entanglement, shown in **(c)**. All adjacent stations are also connected by classical links (not shown).

with two physical qubits: one electron spin (dark purple), which can be used for optically-mediated entanglement, and one nuclear spin (light purple), which has no optical transition but which can use spin-spin interactions to couple to and store quantum information from its local electron spin. This enables the use of “brokered entanglement” [15], where the electron spin serves as a short-term “broker” of entanglement to the longer-term “storage” qubit of the nuclear spin.

In the routerless architecture (Fig. 2a), each of the  $m$  qubit registers first establishes entanglement with the left neighboring node via its electron spin and the corresponding optical mode. This process takes an average number of attempts  $1/p_{\text{distant}}$ . Once successful, this entanglement is swapped to the nuclear spin for storage, at which point the electron spin attempts to establish entanglement with the right neighbor, again requiring an average of  $1/p_{\text{distant}}$  attempts. Thus, the nuclear spin must idle while storing entanglement for an average time  $t_{\text{idle}} \sim t_{\text{distant}}/p_{\text{distant}}$ , where  $t_{\text{distant}}$  is the time needed per attempt of the entanglement protocol, typically limited by the round-trip communication time between the repeater and a detector station. Once this succeeds, a Bell state measurement (BSM) on the joint electron-nuclear spin state teleports entanglement to be shared

across the full link from left to right. This protocol is performed simultaneously and independently on each qubit register.

In contrast, our router architecture (Fig. 2b) defines two “banks” of registers, one with  $\frac{m}{2}$  registers with photonic links to the left, the other with  $\frac{m}{2}$  registers with photonic links to the right. The router connects these two banks using a low-loss  $\frac{m}{2} \times \frac{m}{2}$  switchboard, over which entanglement protocols succeed with probability  $p_{\text{local}} \gg p_{\text{distant}}$ . In this architecture, each qubit register first establishes entanglement with either the left or the right, as determined by their optical connectivity. As in the routerless case, these “successful” registers will then swap entanglement to their nuclear spin. At this point, any successful registers enter a “pairing” stage where registers in opposite banks are paired up and subsequent clock cycles attempt entanglement between electron spins in these pairs. This requires an average number of attempts  $1/p_{\text{local}}$ , taking a time  $t_{\text{idle}} \sim t_{\text{local}}/p_{\text{local}}$ ; here,  $t_{\text{local}}$  is likely dominated by any state initialization required by the entanglement protocol. Any successful but unpaired registers idle, waiting for a successful partner on the opposite side to become available. Once entanglement is formed within a pair, two electron-nuclear spin BSM’s — one at each register — teleport entanglement

to be shared across the full left-right link.

This router architecture has two primary advantages. First, the idling time  $t_{\text{idle}}$  that a storage qubit must hold entanglement can be greatly reduced, decreasing errors due to decoherence. Second, the number of entanglement attempts a register must make while its storage qubit holds entanglement is reduced by a factor  $p_{\text{local}}/p_{\text{distant}}$ , thus sharply reducing the data-qubit decoherence due to broker-qubit entanglement attempts. In the remainder of this article, we quantitatively examine the impact the router has on the performance of a quantum network.

## B. Simulations

We use the NetSquid discrete event simulator [16] to compare the performance of repeaters with and without a router, computing the average rate and fidelity of entanglement distribution for a one-repeater network. In this network, a single repeater station connects Alice and Bob, as shown in Fig. 2 where Alice is the “left node” and Bob is the “right node”. We compare each architecture using the same number of total NV qubit registers  $m$  at the repeater, under the assumption that qubit registers will be a scarce resource in near-term quantum networks. We choose the emission-based Barrett-Kok protocol [4] for our entanglement protocol. The physical parameters of our repeater memories correspond to a realization using photonic integrated circuits discussed below, using experimentally-realized values reported in literature (discussed in Appendix A).

Figure 3a plots the entanglement distribution rates for both repeater architectures for various link distances as a function of the number of qubit registers  $m$  at the repeater node. For the routerless case, as expected since the qubit registers operate independently, the rate scales linearly with  $m$ . For low  $m$ , the router exhibits comparatively lower rates; however, as  $m$  increases, the difference between the two protocols decreases, such that in the limit of large  $m$  the two architectures perform comparably. This difference can be attributed to mismatches in the number of successful entanglements in Alices and Bobs banks after a given clock cycle. The delay in resolving these mismatches, the number of which scales with  $\sqrt{m}$ , lowers the rate of the router below the linear scaling of the routerless architecture. However, the fractional impact of this effect on the rate is reduced for large  $m$ , and the rate of the router approaches the routerless rate.

Figure 3b plots the infidelity of the distributed entanglement for repeaters with and without a router. We consider three sources of infidelities in the distributed entanglement. The first source of infidelity is the typical depolarizing and dephasing noise experienced independently by the electron and nuclear spins, as characterized by their  $T_1$  and  $T_2$  coherence times. We model this noise

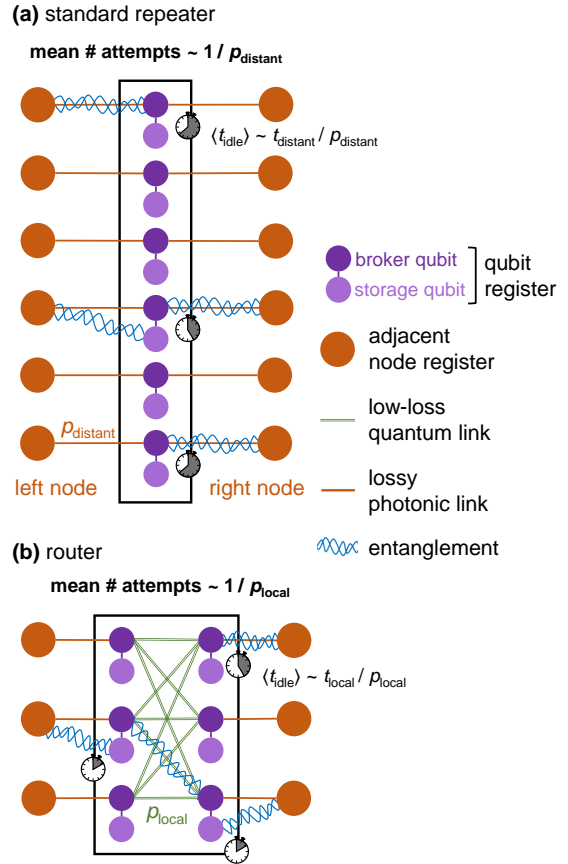


FIG. 2. Abstract representation of a 2-port standard repeater and a 2-port router in a quantum network. Each repeater node hosts  $m$  qubit registers, each of which here is formed by an NV center in diamond comprising a optically active electron spin (dark purple) coupled to a long-coherence nuclear spin (light purple), where the former serves as a broker to store entanglement in the latter. Multiple optical modes can be transmitted through the same physical link, e.g. via temporal or spectral multiplexing. (a) In a standard routerless repeater, each qubit register has lossy photonic links to registers at adjacent network nodes on both the left and the right. (b) In our router architecture, each qubit register has lossy links to only one of the left or right neighbors; however, the repeater node contains local, low-loss quantum channels that enable entanglement generation between all registers in the left bank and all registers in the right bank. As a result, the mean time a storage qubit must idle  $t_{\text{idle}}$  while holding entanglement is shorter with a router.

on a qubit after time  $t$  as:

$$\rho = \begin{pmatrix} 1 - \rho_{11} & \rho_{01} \\ \rho_{01}^* & \rho_{11} \end{pmatrix} \mapsto \begin{pmatrix} 1 - \rho_{11}e^{-t/T_1} & \rho_{01}e^{-t/T_2} \\ \rho_{10}^*e^{-t/T_2} & \rho_{11}e^{-t/T_1} \end{pmatrix}. \quad (1)$$

For a repeater with no router, adding additional registers does not affect the amount of time an individual register must store entanglement; thus, increased multiplexing does not reduce this decoherence channel. However, for a repeater with a router, the number of registers

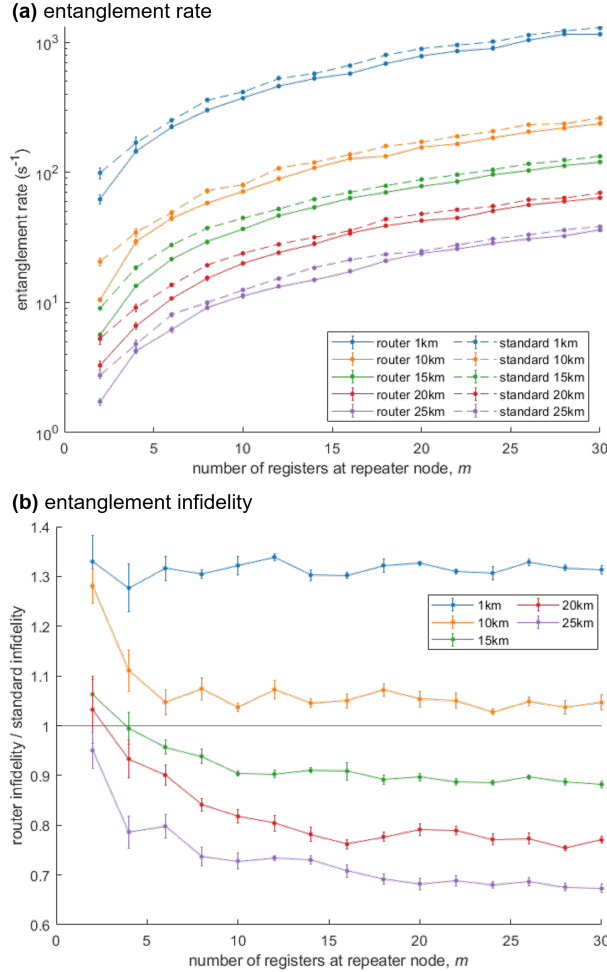


FIG. 3. Simulation results for different repeater node configurations. Each data point is the result of 5 independent simulations. The average rates and infidelities are plotted, with the standard error of the mean shown as the error bars. The lengths (1km, 10km, 15km, 20km, 25km) refer to the distance  $L$  between the repeater node and the detector station. **(a)** As expected, the rate of entanglement generation increases with the number of repeater qubit registers ( $m$ ), as expected. The entanglement rate of the router architecture is slightly lower than the entanglement rate of the standard repeater, and the difference decreases as the size of the repeater increases. **(b)** The fidelity of entanglement generated by the router is higher than that of the standard repeater when the distance  $L$  is sufficiently large. The fidelity of entanglement generated by the router improves as  $m$  increases, whereas that of the standard repeater does not. This causes the infidelity ratio to decrease as  $m$  increases. The infidelity ratio can be arbitrarily small for sufficiently large  $L$  and  $m$ .

has a dramatic effect on the fidelity. This observation can be understood by considering the mean idling time for a memory in this scheme, which is determined by the number of clock cycles a given register in the Alice (Bob) bank must idle after establishing entanglement on its respective side of the link before a register in the Bob (Alice) bank also succeeds and is available for the pairing

stage of the protocol. This maps to the success mismatch problem discussed earlier; as such, in the limit of large  $m$ , most successful registers will be paired with a register in the opposite bank with every clock cycle, such that the idling time approaches the duration of a single such cycle. In contrast, with no router, a register must idle for on average  $1/p_{\text{distant}} \gg 1$  cycles. Thus, the addition of a router reduces the infidelity from this channel by a factor that approaches  $p_{\text{distant}}$ .

The second source of error stems from coupling between the nitrogen nuclear spin and the NV electron spin. In particular, each excitation of the electron spin used to generate spin-photon entanglement in the Barrett-Kok protocol generates noise that decoheres the qubit stored in the nuclear spin. We can model this interaction-induced noise on the nuclear spin as [14]:

$$\rho \mapsto (1 - a - b)\rho + aZ\rho Z + b\frac{\mathbb{I}}{2}, \quad (2)$$

where the dephasing  $a \approx 1/4000$  and the depolarization  $b \approx 1/5000$  for NV centers. Note that for other systems with stronger electron-nuclear spin coupling such as silicon vacancy centers in diamond [17], this effect may be stronger. For both architectures, after a register has generated one entanglement link, it stores that entanglement in the nuclear spin while its electron spin attempts to generate entanglement on the other side — either directly to Bob in the case with no router, or to the opposite bank when using a router. In either case, each failed attempt decreases the fidelity of the final Alice-Bob EPR pair. Without a router, the mean number of failed attempts is equal to  $1/p_{\text{distant}}$ ; with a router, this number is instead  $1/p_{\text{local}}$ , dramatically reducing the infidelity from this effect.

The third source of infidelity comes from imperfect two-qubit gates and electron spin readout. The proposed router needs to perform twice as many two-qubit gates and readouts for each distributed EPR pair as a standard repeater. The cumulative infidelity of these operations is independent of  $m$ ,  $p_{\text{distant}}$ , and  $p_{\text{local}}$ . When the link between adjacent nodes is short, these operations dominate the infidelity of the Alice-Bob EPR pair, disadvantaging the router. However, when the link becomes lossier, the previous two sources of infidelity dominate, causing the router to outperform the standard repeater in entanglement fidelity.

### III. DISCUSSION

Though the complete bipartite connectivity of hybrid repeaters may appear challenging to implement, a router can be added to a standard multiplexed repeater with relatively little physical resource overhead. Figure 4 illustrates one such realization using photonic integrated circuits (PICs). Quantum registers are integrated onto PICs that contain an array of Mach-Zehnder interferome-

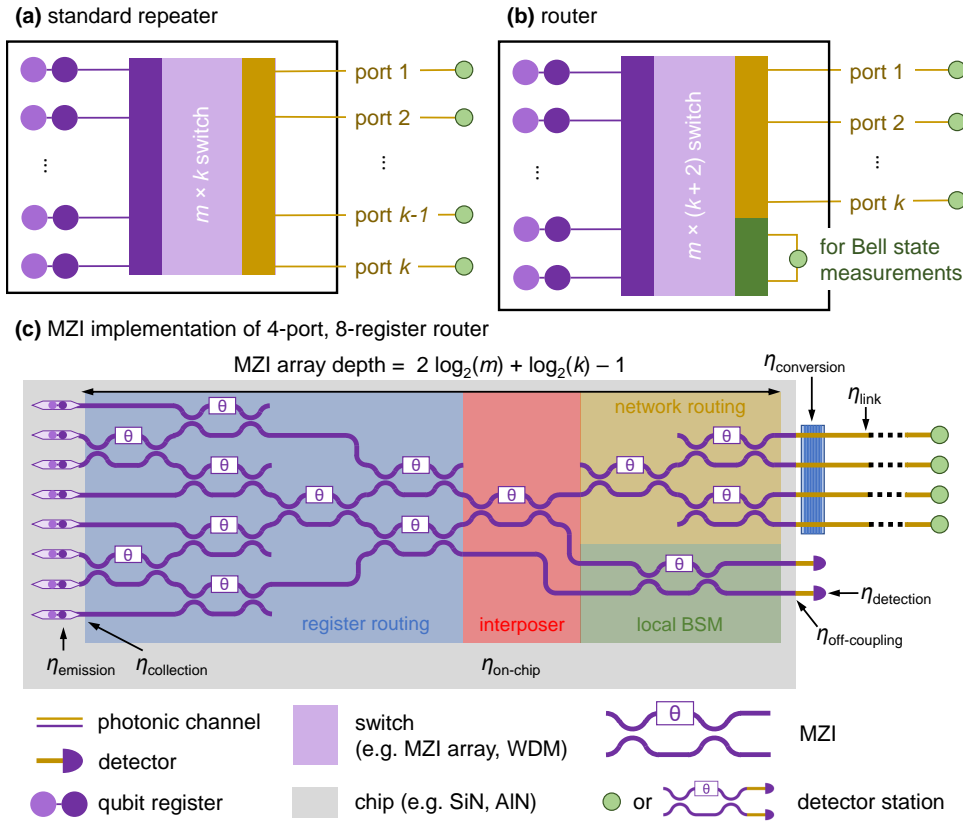


FIG. 4. Potential physical realization of  $k$ -port repeater nodes with  $m$  repeater qubit registers. The main component of our proposed router architecture is a photonic switch that provides all-to-all connectivity from ports on one side of the switch to ports on the other side. Photonic switches can take the form of a tree of Mach-Zehnder interferometers (MZIs) when the modes (Fig. 2) are temporally multiplexed, or a wavelength-division multiplexer when the modes are spectrally multiplexed. (a) A standard (routerless) repeater can be constructed using an  $m \times k$  switch that connects all  $m$  repeater registers with the  $k$  links that go to other nodes in the network. (b) A router can be constructed using an  $m \times (k + 2)$  switch. Photons emitted by the  $m$  repeater registers can travel to the  $k$  links that go to other nodes in the network, or they can be sent to a local detector station for local entanglement generation. (c) A  $k = 4$ -port,  $m = 8$ -register router can be implemented using an MZI array of depth  $\log_2(m^2k/2)$ , comprising a register routing layer (depth  $2\log_2(m/2)$ ), an interposer for routing from local to distant connections (depth 1), a network routing layer (depth  $\log_2(k)$ ), and a local BSM layer (depth 1). The ends of the MZI array are coupled either directly to detectors for the local BSMs or a frequency conversion stage followed by fiber links to distant detector stations for networking. All losses considered in our simulations are shown here.

ters (MZIs) [18], forming a fast switching network to connect any register to any output channel. For a standard multiplexed  $k$ -port repeater with no local connectivity, this requires an  $m \times k$  switch to connect  $m$  repeaters to any of the possible  $k$  neighbors in the network, as shown in Fig. 4a. However, a router can be embedded in this architecture by extending this to an  $m \times (k + 2)$  switch. The additional two ports lead to a detector station as shown in Fig. 4b, thus enabling photon-mediated entanglement between any two registers in the repeater. Since typical single photon detectors have dead times of a few tens of nanoseconds, a single pair of detectors could facilitate many attempts at local entanglement in a single repeater clock cycle, which may be hundreds of microseconds long depending on the length of the link being connected. The additional complexity involved in adding these two additional channels is small, making this ap-

proach an attractive option for implementing high local connectivity.

On a PIC, the  $m \times k$  switch required for the routerless repeater can be realized on an MZI array of depth  $\log_2(m) + \log_2(k)$  [19]. However, this architecture does not permit simultaneous routing from multiple memories, which is desired for the local entanglement operations used in the quantum router. In Fig. 4c we present an architecture that permits arbitrary  $m \times k$  routing for connecting registers to the network, allows simultaneous routing from two memories to perform Bell state measurements for local entanglement generation, and maintains  $\mathcal{O}(\log m)$  scaling of the array depth. The addition of a 1-layer interposer permits routing between the network and a Bell state measurement setup for local entanglement generation. The simulations presented in Fig. 3 utilize this architecture assuming an aluminum nitride

(AlN) based photonic chip; alternative implementations include using silicon nitride (SiN) [20] or lithium niobate (LN) [11]. Additional improvements include integrating detectors on-chip [21] to eliminate the off-chip coupling inefficiency for local measurements and integrating the frequency conversion stage on-chip, which is feasible in highly nonlinear materials such as LN [22].

This platform is an attractive path for realizing recent proposals for on-chip polarization-to-spin based networking [23]. The PIC implementation presents an additional benefit if the links to Alice and Bob have different transmissivities. Since both the rate and fidelity of entanglement distribution are limited by the difference in the time needed to establish entanglement with both Alice and Bob, the repeater in Fig. 2b (with equal numbers of registers in the Alice and Bob banks) will be limited by the lossier side. In contrast, the PIC implementation allows dynamic allocation of registers to Alice and Bob to balance the rates of entanglement generation. This optimizes the entanglement rate by effectively increasing the multiplexing on lossier ports, and optimizes the entanglement fidelity by preventing a build-up of idling registers on a lower-loss port. Finally, dynamic memory allocation is also of great importance for managing entanglement flow in general 2D quantum network geometries [24].

In conclusion, the inclusion of a "photonic switchboard" enables a routered repeater to provide higher-fidelity entanglement distribution compared to routerless repeater architectures, without significant loss to the entanglement distribution rate. An important next step will be to exploit the local connectivity for entanglement

distillation [25] and local error correction [26] to further improve the fidelity of generated EPR pairs. These options allow the entanglement rate to be traded off for entanglement fidelity, without affecting the architecture of the repeater itself. While we demonstrated these results assuming parameters observed for NV centers in diamond, the improvements are agnostic to the entanglement protocol, and should apply generally to quantum networks. Our findings emphasize the importance of local connectivity in designing quantum repeaters and pave the way for high-efficiency, scalable quantum networks.

#### IV. ACKNOWLEDGEMENTS

Y.L. acknowledges funding support by the MIT School of Engineering's SuperUROP program. E.B. is supported by a NASA Space Technology Research Fellowship and the NSF Center for Ultracold Atoms (CUA). D.E. acknowledges support from the NSF EFRI-ACQUIRE program Scalable Quantum Communications with Error-Corrected Semiconductor Qubits. We also thank Ian Christen and Kevin Chen for valuable discussions.

#### V. AUTHOR CONTRIBUTIONS

Y.L. and E.B. designed and performed the simulations. D.E. conceived the idea. A.D. and S.W. developed the NetSquid simulator. All authors contributed to writing and revising the manuscript.

---

[1] B. Hensen, H. Bernien, A. E. Dréau, A. Reiserer, N. Kalb, M. S. Blok, J. Ruitenberg, R. F. L. Vermeulen, R. N. Schouten, C. Abellán, W. Amaya, V. Pruneri, M. W. Mitchell, M. Markham, D. J. Twitchen, D. Elkouss, S. Wehner, T. H. Taminiau, and R. Hanson, "Loophole-free Bell inequality violation using electron spins separated by 1.3 kilometres," *Nature*, vol. 526, no. 7575, pp. 682–686, 2015.

[2] M. Takeoka, S. Guha, and M. M. Wilde, "Fundamental rate-loss tradeoff for optical quantum key distribution," *Nature Communications*, vol. 5, p. 5235, Oct 2014.

[3] H.-J. Briegel, W. Dür, J. I. Cirac, and P. Zoller, "Quantum repeaters: The role of imperfect local operations in quantum communication," *Phys. Rev. Lett.*, vol. 81, pp. 5932–5935, Dec 1998.

[4] S. D. Barrett and P. Kok, "Efficient high-fidelity quantum computation using matter qubits and linear optics," *Phys. Rev. A*, vol. 71, p. 060310, Jun 2005.

[5] C. Cabrillo, J. I. Cirac, P. García-Fernández, and P. Zoller, "Creation of entangled states of distant atoms by interference," *Phys. Rev. A*, vol. 59, pp. 1025–1033, Feb 1999.

[6] P. C. Humphreys, N. Kalb, J. P. J. Morits, R. N. Schouten, R. F. L. Vermeulen, D. J. Twitchen, M. Markham, and R. Hanson, "Deterministic delivery of remote entanglement on a quantum network," *Nature*, vol. 558, no. 7709, pp. 268–273, 2018.

[7] M. K. Bhaskar, R. Riedinger, B. Machielse, D. S. Levonian, C. T. Nguyen, E. N. Knall, H. Park, D. Englund, M. Lončar, D. D. Sukachev, and M. D. Lukin, "Experimental demonstration of memory-enhanced quantum communication," *Nature*, vol. 580, pp. 60–64, Apr 2020.

[8] L.-M. Duan and H. J. Kimble, "Scalable Photonic Quantum Computation through Cavity-Assisted Interactions," *Phys. Rev. Lett.*, vol. 92, p. 127902, Mar 2004.

[9] W. J. Munro, K. A. Harrison, A. M. Stephens, S. J. Devitt, and K. Nemoto, "From quantum multiplexing to high-performance quantum networking," *Nature Photonics*, vol. 4, no. 11, pp. 792–796, 2010.

[10] S. B. van Dam, P. C. Humphreys, F. Rozpedek, S. Wehner, and R. Hanson, "Multiplexed entanglement generation over quantum networks using multi-qubit nodes," *Quantum Science and Technology*, vol. 2, p. 034002, Jun 2017.

[11] B. Desiatov, A. Shams-Ansari, M. Zhang, C. Wang, and M. Lončar, "Ultra-low-loss integrated visible photonics using thin-film lithium niobate," *Optica*, vol. 6, pp. 380–384, Mar 2019.

[12] N. H. Wan, T.-J. Lu, K. C. Chen, M. P. Walsh, M. E. Trusheim, L. D. Santis, E. A. Bersin, I. B. Harris, S. L.

Mouradian, I. R. Christen, E. S. Bielejec, and D. Englund, "Large-scale integration of near-indistinguishable artificial atoms in hybrid photonic circuits," 2019.

[13] A. Dahlberg, M. Skrzypczyk, T. Coopmans, L. Wubben, F. Rozpedek, M. Pompili, A. Stolk, P. Pawełczak, R. Knegjens, J. de Oliveira Filho, and et al., "A Link Layer Protocol for Quantum Networks," in *Proceedings of the ACM Special Interest Group on Data Communication, SIGCOMM 19*, (New York, NY, USA), p. 159173, Association for Computing Machinery, 2019.

[14] F. Rozpedek, R. Yehia, K. Goodenough, M. Ruf, P. C. Humphreys, R. Hanson, S. Wehner, and D. Elkouss, "Near-term quantum-repeater experiments with nitrogen-vacancy centers: Overcoming the limitations of direct transmission," *Physical Review A*, vol. 99, May 2019.

[15] S. C. Benjamin, D. E. Browne, J. Fitzsimons, and J. J. L. Morton, "Brokered graph-state quantum computation," *New Journal of Physics*, vol. 8, pp. 141–141, aug 2006.

[16] "NetSquid." <https://netsquid.org/>, 2019.

[17] C. T. Nguyen, D. D. Sukachev, M. K. Bhaskar, B. Machielse, D. S. Levonian, E. N. Knall, P. Stroganov, R. Riedinger, H. Park, M. Lončar, and M. D. Lukin, "Quantum network nodes based on diamond qubits with an efficient nanophotonic interface," *Phys. Rev. Lett.*, vol. 123, p. 183602, Oct 2019.

[18] N. C. Harris, G. R. Steinbrecher, M. Prabhu, Y. Lahini, J. Mower, D. Bunandar, C. Chen, F. N. C. Wong, T. Baehr-Jones, M. Hochberg, S. Lloyd, and D. Englund, "Quantum transport simulations in a programmable nanophotonic processor," *Nature Photonics*, vol. 11, no. 7, pp. 447–452, 2017.

[19] B. G. Lee and N. Dupuis, "Silicon photonic switch fabrics: Technology and architecture," *J. Lightwave Technol.*, vol. 37, pp. 6–20, Jan 2019.

[20] S. L. Mouradian, T. Schröder, C. B. Poitras, L. Li, J. Goldstein, E. H. Chen, M. Walsh, J. Cardenas, M. L. Markham, D. J. Twitchen, M. Lipson, and D. Englund, "Scalable integration of long-lived quantum memories into a photonic circuit," *Phys. Rev. X*, vol. 5, p. 031009, Jul 2015.

[21] F. Najafi, J. Mower, N. C. Harris, F. Bellei, A. Dane, C. Lee, X. Hu, P. Kharel, F. Marsili, S. Assefa, K. K. Berggren, and D. Englund, "On-chip detection of non-classical light by scalable integration of single-photon detectors," *Nature Communications*, vol. 6, p. 5873, Jan 2015.

[22] C. Wang, C. Langrock, A. Marandi, M. Jankowski, M. Zhang, B. Desiatov, M. M. Fejer, and M. Lončar, "Ultrahigh-efficiency wavelength conversion in nanophotonic periodically poled lithium niobate waveguides," *Optica*, vol. 5, pp. 1438–1441, Nov 2018.

[23] K. C. Chen, E. Bersin, and D. Englund, "A polarization encoded photon-to-spin interface," 2020.

[24] M. Pant, H. Krovi, D. Towsley, L. Tassiulas, L. Jiang, P. Basu, D. Englund, and S. Guha, "Routing entanglement in the quantum internet," *npj Quantum Information*, vol. 5, p. 25, Mar 2019.

[25] N. Kalb, A. A. Reiserer, P. C. Humphreys, J. J. W. Bakermans, S. J. Kamerling, N. H. Nickerson, S. C. Benjamin, D. J. Twitchen, M. Markham, and R. Hanson, "Entanglement distillation between solid-state quantum network nodes," *Science*, vol. 356, p. 928932, Jun 2017.

[26] J. Cramer, N. Kalb, M. A. Rol, B. Hensen, M. S. Blok, M. Markham, D. J. Twitchen, R. Hanson, and T. H. Taminiau, "Repeated quantum error correction on a continuously encoded qubit by real-time feedback," *Nature Communications*, vol. 7, p. 11526, May 2016.

[27] J. Notaros, F. Pavanello, M. Wade, C. Gentry, A. Atabaki, L. Alloatti, R. Ram, and M. Popovic, "Ultra-Efficient CMOS Fiber-to-Chip Grating Couplers," p. M2I.5, 01 2016.

[28] T.-J. Lu, M. Fanto, H. Choi, P. Thomas, J. Steidle, S. Mouradian, W. Kong, D. Zhu, H. Moon, K. Berggren, J. Kim, M. Soltani, S. Preble, and D. Englund, "Aluminum nitride integrated photonics platform for the ultraviolet to visible spectrum," *Optics Express*, vol. 26, p. 11147, 04 2018.

[29] L. Li, T. Schröder, E. H. Chen, M. Walsh, I. Bayn, J. Goldstein, O. Gaathon, M. E. Trusheim, M. Lu, J. Mower, M. Cotlet, M. L. Markham, D. J. Twitchen, and D. Englund, "Coherent spin control of a nanocavity-enhanced qubit in diamond," *Nature Communications*, vol. 6, no. 1, p. 6173, 2015.

[30] Y. Yu, F. Ma, X.-Y. Luo, B. Jing, P.-F. Sun, R.-Z. Fang, C.-W. Yang, H. Liu, M.-Y. Zheng, X.-P. Xie, W.-J. Zhang, L.-X. You, Z. Wang, T.-Y. Chen, Q. Zhang, X.-H. Bao, and J.-W. Pan, "Entanglement of two quantum memories via fibres over dozens of kilometres," *Nature*, vol. 578, no. 7794, pp. 240–245, 2020.

[31] H. Le Jeannic, V. B. Verma, A. Cavaillès, F. Marsili, M. D. Shaw, K. Huang, O. Morin, S. W. Nam, and J. Laurat, "High-efficiency ws1 superconducting nanowire single-photon detectors for quantum state engineering in the near infrared," *Optics Letters*, vol. 41, p. 5341, Nov 2016.

[32] M. Abobeih, J. Cramer, M. Bakker, N. Kalb, D. Twitchen, M. Markham, and T. Taminiau, "One-second coherence for a single electron spin coupled to a multi-qubit nuclear-spin environment," *Nature Communications*, vol. 9, p. 2552, 2018.

[33] C. E. Bradley, J. Randall, M. H. Abobeih, R. C. Berrevoets, M. J. Degen, M. A. Bakker, M. Markham, D. J. Twitchen, and T. H. Taminiau, "A ten-qubit solid-state spin register with quantum memory up to one minute," *Phys. Rev. X*, vol. 9, p. 031045, Sep 2019.

[34] A. Reiserer, N. Kalb, M. S. Blok, K. J. M. van Bemmel, T. H. Taminiau, R. Hanson, D. J. Twitchen, and M. Markham, "Robust Quantum-Network Memory Using Decoherence-Protected Subspaces of Nuclear Spins," *Phys. Rev. X*, vol. 6, p. 021040, Jun 2016.

[35] N. Kalb, P. C. Humphreys, J. J. Slim, and R. Hanson, "Dephasing mechanisms of diamond-based nuclear-spin memories for quantum networks," *Phys. Rev. A*, vol. 97, p. 062330, Jun 2018.

TABLE I. State-of-the-art parameters used in simulations. Noise from two-qubit gates and electron spin readout are modeled as depolarization; noise from memory-photon state preparation is modeled as dephasing.

Parameter	Value	Description
$\eta_{\text{emission}}$	0.66 [29]	Fraction of NV emissions that are coherent
$\eta_{\text{collection}}$	0.83 [20]	Collection efficiency from NVs
$\eta_{\text{local}}$	(Refer to text.)	Efficiency of local routing
$\eta_{\text{conversion}}$	0.33 [30]	Efficiency of frequency conversion
$\eta_{\text{detection}}$	0.93 [31]	Detector efficiency
$d$	$100\text{ s}^{-1}$	Detector dark count rate
$T_1^e$	3600 s [32]	Electron depolarizing time
$T_2^e$	1.58 s [32]	Electron dephasing time
$T_1^n$	$> 86400\text{s}$	Nuclear depolarizing time (too long to measure accurately)
$T_2^n$	63 s [33]	Nuclear dephasing time
$a$	$1/4000$ [34, 35]	Interaction-induced dephasing
$b$	$1/5000$ [34]	Interaction-induced depolarization
$\alpha$	$0.041\text{ km}^{-1}$	Fiber loss (0.18 dB/km at telecom wavelengths)
$F_{\text{gate}}$	0.98 [25]	Fidelity of two-qubit gates
$F_{\text{readout}}$	0.9998 [7]	Readout fidelity from electron spin
$F_{\text{initialization}}$	0.99 [1]	Fidelity of memory-photon state preparation

## Appendix A: Simulation Parameters

The physical parameters of our repeater memories correspond to experimentally-realized values reported in literature, detailed in Table I. In particular, these simulations consider a number of loss mechanisms. Only a fraction  $\eta_{\text{emission}}$  of the NV emissions are coherent and thus usable for quantum networking, with the remainder being scattered into an incoherent phonon-sideband. The NV also emits into a wide range of spatial modes, yielding a limited collection efficiency  $\eta_{\text{collection}}$ . Local routing at the repeater is performed with efficiency  $\eta_{\text{local}}$ . The NV's visible emission wavelength experiences high losses of around 8 dB/km in fiber [1]; as a result, long-distance networking applications require a frequency

downconversion step to telecom wavelengths with efficiency  $\eta_{\text{conversion}}$ . The primary source of loss is scattering in the optical fiber that links the network nodes. This loss scales exponentially with the link length  $L$ , giving transmission efficiency  $\eta_{\text{link}} = e^{-\alpha L}$ . The transmission losses  $\eta_{\text{transmission}}$  labeled in Fig. 4 combine contributions from frequency downconversion and scattering losses in the fiber. Finally, the single photon detectors used to herald entanglement have a finite detection efficiency  $\eta_{\text{detection}}$  and dark count rate  $d$ .

There are two components to the efficiency of local routing  $\eta_{\text{local}}$ : off-chip coupling efficiencies  $\eta_{\text{off-coupling}} = 0.92$  [27] and on-chip propagation efficiencies  $\eta_{\text{on-chip}} = 0.9963$  per MZI. To compute the latter, we assume that AlN has a loss of 5.3 dB/cm with a footprint of 30  $\mu\text{m}$  per MZI [28].